Journal of Fluids and Structures (2001) **15,** 1105–1121
doi:10.1006/jfls.2000.0371, available online at http://www.idealibrary.com on IDEAL®

ROUTE TO SURGE FOR A THROTTLED COMPRESSOR — A NUMERICAL STUDY

O. Schmidtmann†

Fachbereich Mathematik und Informatik, Universität Bremen, Zentrum für Technomathematik PF 33 04 40, D-28334 Bremen, Germany

AND

J. M. Anders

BMW Rolls–Royce AeroEngines Dahlewitz, Eschenweg 11 D-15827 Dahlewitz, Germany

(Received 18 March 1999, and in final form 22 October 2000)

Aerodynamic instabilities of axial compressors are investigated numerically and compared with experimental results. The compressor flow in the interblade-row spaces is simulated by means of 2-D Euler equations while the blade rows are modelled as quasi-steady actuator disks. The coupling of different unbladed regions of the compressor by actuator disks, which is characterized by the influence of stator and rotor, is captured in terms of conservation laws and source terms by means of compressor characteristics. At inflow and outflow nonreflecting boundary conditions are used in order to avoid any nonphysical reflections at the boundary. Numerically simulating this model for selected initial and boundary conditions, we observe that for increasing values of the imposed exit pressure the compressor flow undergoes several qualitative changes. At some critical value of exit pressure a primary stable steady state losses stability to several coexisting time-periodic states with a number of rotating stall cells. While for these time-periodic states the mass flow does not depend on time, all solution branches lead finally to surge, i.e., to states with an oscillation of mass flow in time if the exit pressure is sufficiently large. In addition, the numerical results are compared with experimental measurements.

1. INTRODUCTION

Axial compression systems which are part of turbomachines are designed to transfer energy from the rotor to the fluid resulting in an overall rise of its enthalpy and an associated pressure rise. The fluid is guided in a steady flow through an annular duct, where by rechannelling the fluid by rotor and stator blades in different stages kinetic energy is transferred into internal energy. The reverse occurs in a turbine, which delivers kinetic energy in exchange for thermal energy of the fluid resulting in a reduction of its enthalpy and an associated pressure drop. An overview of turbomachinary theory is given for example by Cordes (1963) and Lewis (1996).

It is well known from experimental measurement that if the mass flow through the compressor is sufficiently large there exists a stable steady state. If the mass flow is reduced, for example by throttling the compressor, the steady flow losses stability to a

† Present address: EADS Airbus GMBH, Kreetslag 10, D-21129 Hamburg, Germany.

0889–9746/01/081105 + 17 $35.00/0

time-dependent state. Two main types of aerodynamic flow instabilities in compressors are well known: rotating stall and surge (Gravdahl & Egeland 1999). Rotating stall is a propagation of disturbances in circumferential direction and located to a single rotor or stator. Explanations of rotating stall mechanisms were given by Emmons *et al.* (1955). Surge is an instability of the flow in the whole compressor and is characterized by flow oscillations through the compressor in axial direction with a low frequency compared to rotating stall. In the compressor characteristic it is represented as a limit cycle. These instabilities limit the range of operation for compressors and lead to a reduction of its capacity or may destroy the compressor. A central problem for design of turbomachines is to understand and to model the inception of these flow instabilities and to develop perturbation resistant aerodynamic design features. Instabilities may be avoided by using control systems to prevent the operating point of the compressor to enter the unstable region in the compressor characteristic or by stabilizing unstable states which is known as active surge/stall control (Gravdahl 1998). The essential aim of the theoretical investigation is to explain stall and surge mechanisms and to identify the location of inception points, what is still an unsolved problem. To this end a number of compressor models have been developed and numerical calculations of these models have been done in order to investigate compressor instabilities. In some sense still a step further goes a bifurcation, or qualitative, analysis, by which, in contrast to simply simulating a system for selected initial conditions, one tries to get an overview of the attractor structure of the model, i.e., of the set of possible time-asymptotic states. The main objective of a bifurcation analysis is the determination of the time-asymptotic states for a given set of external control parameters and the characterization of the qualitative changes of these states (bifurcations) that occur when the control parameters are varied. The details of the relaxation towards the attractors, as for example the temporal evolution of instabilities, are of lesser interest here. This approach will be investigated in the present paper.

The flows in turbocompressors are highly irregular and turbulent. The full description of such flows by direct numerical calculation of the Navier–Stokes equations (NSE) is not a realistic task. It is beyond analytic methods and beyond the possibilities of computers at the present time and in the foreseeable future. For this reason a number of turbulence and boundary layer models are frequently used if the spatial and temporal resolution of the simulation is not able to resolve the whole range of turbulence in space and time (Wilcox 1993; Merz *et al.*, 1996). A more realistic task is the approximate description of large-scale behaviour of compressor flows where the viscous effects in the blade passages are modelled while the viscous effects in the unbladed regions are neglected. This is justified since Reynolds numbers, Re, in high-speed compressors are very large ($\mathrm{Re} \approx 10^6$). Therefore, in order to model the flow through a multistage high-speed compressor Euler equations of gas dynamics (Anderson *et al.*, 1984; LeVeque 1990) are combined frequently with an external forcing to model the influence of stator or rotor or the transfer from bladed to unbladed regions and *vice versa* in the compressor.

The majority of compressor models simulate the compressor flow by a low-dimensional system of ordinary differential equations (ODE). In 1976 Greitzer and Moore started a systematic investigation of the stability behaviour of steady-state solutions in axial compressors (Greitzer 1976*a*, *b*, 1981; Greitzer & Moore 1986; Moore & Greitzer 1986). Beginning with a rather simple model, namely a low-dimensional nonlinear system of ODEs, they included more and more details of the geometry of the compressor. These models are able to describe the inception of surge oscillations, while rotating stall is observed as a pressure drop. Bifurcation theory has been applied by McCaughan (1989) to the low-dimensional Greitzer (1976*a*) model and by Brøns (1988, 1990) to the model of Greitzer & Moore (1986). It has been shown that surge occurs after a Hopf bifurcation where

Greitzer's B parameter is changed to control the system. Bifurcation theory has been applied also by Liaw & Abed (1996) to derive control methods for the Moore–Greitzer model.

More recently, Euler equations of gas dynamics have been used to model the flow in compressors. It has been found that surge which is a one-dimensional compression system response occurs after an initial period of rotating stall (Day 1994). There are two types of mechanisms leading to rotating stall which result from an initial flow field instability for a throttled compressor with fixed rotation speed. Spike type stall inception, i.e., distinctly localized disturbances are observed in one individual blade passage and propagate in a neighbouring blade passage (Day 1993). Another type of stall, modal-type stall inception, is caused by flow field disturbances, whose lengthscales are large and the propagation speed is small compared to spikes (McDougall *et al.*, 1990; Longley 1994). In 1995 a two-dimensional compressor model has been introduced by Breuer (1995, 1996) to investigate flow instabilities. The influence of blading has been modelled by special source terms. A very good correspondence between calculated and measured data of the complex flows has been observed. Imposing a special force, which describes the influence of blades, Longley (1996, 1997) and Demargne & Longley (1997) introduced a model, which combines 1-D simulations in blade passages and 2-D simulations in the unbladed regions. A main result of their investigation is that varying the mass flow does more influence the stability of the flow than varying the blade angles.

In the present paper, we continue the study of Breuer and Longley by identifying system parameters which influence the solution behaviour of the model. By systematically changing these parameters we are able to describe a scenario for the transition from steady-state flow to surge. The compressor model developed here is concerned with the approximate description of large-scale long-term behaviour of compressor flows. The flow is simulated in unbladed regions with 2-D Euler equations of gas dynamics, while rotor and stator are modelled as actuator disks. The paper is structured as follows. In Section 2, we introduce the Euler equations of gas dynamics, while in Section 3 we describe the model for a multistage axial compressor under consideration. Then in Section 4, we present our numerical results. We describe the qualitative changes of the flow with increasing exit pressure. In Section 5, we compare our numerical results with measured data. Section 6, finally, contains a brief conclusion.

2. BASIC EQUATIONS OF GAS DYNAMICS

We start from the Euler equations for a compressible, inviscid, ideal gas with constant material properties [cf., e.g., Anderson *et al.* (1984), Courant & Friedrichs (1976)],

$$\frac{\partial \rho}{\partial t} + \operatorname{div}(\rho \mathbf{u}) = f_\rho, \tag{1}$$

$$\rho\left(\frac{\partial \mathbf{u}}{\partial t} + (\mathbf{u}\cdot\nabla)\mathbf{u}\right) + \nabla p = f_{\mathbf{u}}, \tag{2}$$

$$\frac{\partial E}{\partial t} + \operatorname{div}(\mathbf{u}(E+p)) = f_E, \tag{3}$$

where the unknown functions are the density ρ, the gas velocity $\mathbf{u}$, the total energy of the gas E and its pressure p; f_ρ, $f_{\mathbf{u}}$, f_E are source terms for mass, momentum and energy, respectively.

The total energy E of the gas is decomposed into a sum of kinetic and internal energy

$$E = \tfrac{1}{2}\rho \mathbf{u}^2 + \rho e,$$

where e is the specific internal energy, which is given as a function of both density ρ and pressure p by the equation of state

$$e = e(\rho, p).$$

We assume the gas to be ideal that means the equation of state takes the form

$$p = \mathscr{R}\rho T,$$

where $\mathscr{R}$ is a constant and the internal energy $e = e(T)$ is a function of temperature T. In addition, we assume that the gas is polytropic, i.e., e is proportional to T

$$e = c_v T,$$

where c_v is the specific heat at constant volume. The enthalpy h

$$h = e + \frac{p}{\rho}$$

is a function of T,

$$h = c_p T.$$

For a polytropic gas the specific heat at constant pressure c_p is also assumed to be constant. The equation of state for a polytropic gas takes the form

$$e = c_v T = \left(\frac{c_v}{R}\right)\frac{p}{\rho} = \frac{p}{(\gamma - 1)\rho},$$

where $\mathscr{R} = c_p - c_v$ is the gas constant and $\gamma = c_p/c_v$ is the ratio of specific heats and the pressure p is given by

$$p = (\gamma - 1)\rho e. \tag{4}$$

Equations (1)–(3) are completed by initial and boundary conditions upon ρ, $\mathbf{u}$ and E.

3. COMPRESSOR MODEL

We have investigated the flow in a two-stage high-speed compressor. The domain of calculation consists of five single unbladed regions, one at the left entrance and one behind every blade row. The domain behind the stator of stage 2 serves as a model for a downstream plenum which plays an important role in the surge behaviour of the compressor (Moore & Greitzer 1986) and it also determines the frequency of the surge oscillations. The geometry as well as the characteristic and the design parameters of the compressor under consideration are described in the Appendix. For the numerical calculation of the flow in the unbladed regions of our model we use a Godunov method with Roe solver by LeVeque (1994, 1997).

The flow in a compressor is influenced by the interaction of several compressor stages, where every single stage consists of one rotor and one stator which are separated by an interblade-row space. The simulation in our model is carried out in these gaps between rotor and stator only, while the influence of rotor and stator is given by transfer functions. For the simulation of the flow between the adjacent blade rows we neglect the radial component of velocity, i.e., the flows are annular and the simulation is two-dimensional. In these unbladed regions, where we use 2-D Euler equations, we restrict ourselves to periodic boundary conditions in the circumferential direction, what is equivalent to considering the motion on a surface of a cylinder. In the axial direction, in order to avoid any nonphysical

reflections at inflow and outflow of the compressor, we use nonreflecting boundary conditions, which have been introduced by Engquist & Majda (1977) and Giles (1990) (see Section 3.1).

The influence of stator and rotor blades, like the transfer of energy from the rotor to the fluid or pressure rise, as well as the interaction of several unbladed regions is simulated by means of transfer functions. The transfer function gives values for velocity, internal energy and density on the left and right boundary of every interblade-row gap at time step $n + 1$ as a function of these quantities at time step n, which we have obtained by means of our simulation. So we take into account the influence of stator and rotor of every single compressor stage without explicitly simulating the flow in a blade row. The transfer functions are obtained from compressor characteristics and conservation laws (see Section 3.2).

3.1. Non-Reflecting Boundary Conditions

To implement boundary conditions at inflow and outflow we transform equations (1)–(3), which are a hyperbolic system of partial differential equations (PDE), for two dimensions into

$$\frac{\partial \mathbf{U}}{\partial t} + A(\mathbf{U})\frac{\partial \mathbf{U}}{\partial x} + B(\mathbf{U})\frac{\partial \mathbf{U}}{\partial y} = \mathbf{0}, \tag{5}$$

where

$$\mathbf{U} = \begin{Bmatrix} \rho \\ u \\ v \\ p \end{Bmatrix}, \quad A(\mathbf{U}) = \begin{bmatrix} u & \rho & 0 & 0 \\ 0 & u & 0 & \rho^{-1} \\ 0 & 0 & u & 0 \\ 0 & \gamma p & 0 & u \end{bmatrix} \quad \text{and} \quad B(\mathbf{U}) = \begin{bmatrix} v & 0 & \rho & 0 \\ 0 & v & 0 & 0 \\ 0 & 0 & v & \rho^{-1} \\ 0 & 0 & \gamma p & v \end{bmatrix}.$$

Equation (5) is called hyperbolic if any real linear combination $\alpha A(\mathbf{U}) + \beta B(\mathbf{U})$ is diagonalizable with distinct real eigenvalues, which depend on $\mathbf{U}$. These eigenvalues determine the direction of characteristic curves, along which the values of certain characteristic variables propagate. Therefore, the values of outgoing characteristic variables are not to be prescribed at the boundary but calculated by extrapolating the corresponding characteristic curves. The values of incoming characteristic variables can be prescribed either in order to control the state of the system or to describe the influence of adjacent interblade-row spaces.

While for an exact formulation of boundary condition it would be necessary to calculate characteristic curves for the nonlinear equation (5), we restrict ourselves because of simplicity to a linearized equation. That means we linearize equation (5) around a given steady-state solution and formulate boundary conditions for perturbations to this solution. In this case characteristic curves are straight lines. In addition, we assume that disturbances propagate in the axial direction only. To prescribe nonreflecting boundary conditions at inflow and outflow of the compressor means to prescribe the values of incoming characteristic curves such that any disturbance leaving the compressor should not be reflected by the boundary.

The linearization of equation (5) around a given steady state $\hat{\mathbf{U}}$ take the form

$$\frac{\partial \tilde{\mathbf{U}}}{\partial t} + A(\hat{\mathbf{U}})\frac{\partial \tilde{\mathbf{U}}}{\partial x} + B(\hat{\mathbf{U}})\frac{\partial \tilde{\mathbf{U}}}{\partial y} = \mathbf{0}, \tag{6}$$

where $\tilde{\mathbf{U}} = (\tilde{\rho}, \tilde{u}, \tilde{v}, \tilde{p})$ is a small disturbance of a solution $\hat{\mathbf{U}} = (\hat{\rho}, \hat{u}, \hat{v}, \hat{p})$ to equation (5). We assume that waves travel in the axial direction only, that means we assume

$$\frac{\partial \tilde{\mathbf{U}}}{\partial y} = \mathbf{0}.$$

Due to the hyperbolicity of equation (6), we can decompose

$$A = R\Lambda R^{-1}, \tag{7}$$

where $\Lambda = \mathrm{diag}(\lambda_1, \lambda_2, \lambda_3, \lambda_4)$ is the diagonal matrix of eigenvalues and $R = [\mathbf{r}_1, \mathbf{r}_2, \mathbf{r}_3, \mathbf{r}_4]$ is the matrix of right eigenvectors with

$$A\mathbf{r}_i = \lambda_i \mathbf{r}_i, \quad i = 1, \ldots, 4.$$

We define characteristic variables

$$\mathbf{c} := R^{-1}\tilde{\mathbf{U}}$$

and using equation (7) gives a linear hyperbolic PDE for $\mathbf{c}$

$$\frac{\partial \mathbf{c}}{\partial t} + \Lambda \frac{\partial \mathbf{c}}{\partial x} = \mathbf{0},$$

which decouples into four scalar PDEs, whose solutions are

$$\mathbf{c}_i(x, t) = \mathbf{c}_i(x - \lambda_i t, 0), \quad i = 1, \ldots, 4.$$

According to the eigenvalues of A for $0 < \hat{u} < c$, which are $\lambda_{1,2} = \hat{u} > 0$, $\lambda_3 = \hat{u} + c > 0$, $\lambda_4 = \hat{u} - c < 0$ (c denotes the speed of sound) the characteristic variables $\mathbf{c}_1, \mathbf{c}_2, \mathbf{c}_3$ describe right-travelling waves and $\mathbf{c}_4$ describes a left-travelling wave. The transformation between characteristic and original variables is given by

$$\begin{Bmatrix} \mathbf{c}_1 \\ \mathbf{c}_2 \\ \mathbf{c}_3 \\ \mathbf{c}_4 \end{Bmatrix} = \begin{bmatrix} -c^2 & 0 & 0 & 1 \\ 0 & 0 & \hat{\rho}c & 0 \\ 0 & \hat{\rho}c & 0 & 1 \\ 0 & -\hat{\rho}c & 0 & 1 \end{bmatrix} \begin{Bmatrix} \tilde{\rho} \\ \tilde{u} \\ \tilde{v} \\ \tilde{p} \end{Bmatrix} \tag{8}$$

and

$$\begin{Bmatrix} \tilde{\rho} \\ \tilde{u} \\ \tilde{v} \\ \tilde{p} \end{Bmatrix} = \begin{bmatrix} -1/c^2 & 0 & 1/2c^2 & 1/2c^2 \\ 0 & 0 & 1/2\hat{\rho}c & -1/2\hat{\rho}c \\ 0 & 1/\hat{\rho}c & 0 & 0 \\ 0 & 0 & 1/2 & 1/2 \end{bmatrix} \begin{Bmatrix} \mathbf{c}_1 \\ \mathbf{c}_2 \\ \mathbf{c}_3 \\ \mathbf{c}_4 \end{Bmatrix}. \tag{9}$$

Since the characteristic variable $\mathbf{c}_4$ at inflow and $\mathbf{c}_1, \mathbf{c}_2, \mathbf{c}_3$ at outflow of every interblade-row gap are calculated by extrapolating characteristic curves and cannot be prescribed from outside the only possibility to prescribe boundary conditions is to specify $\mathbf{c}_1, \mathbf{c}_2, \mathbf{c}_3$ on the left and $\mathbf{c}_4$ on the right side of every interblade-row gap; to impose boundary conditions, which prevent any reflexions of outgoing waves. We therefore set $\mathbf{c}_1, \mathbf{c}_2, \mathbf{c}_3 = \mathbf{0}$ at the inflow and $\mathbf{c}_4 = \mathbf{0}$ at the outflow.

3.2. Transfer Functions

For the coupling of several interblade-row gaps we have to determine ρ, u, v and E at time step $n + 1$ on the right and left boundary of every blade row from values of these variables

at time-step n, which we have obtained by means of our simulation. To this end we have to evaluate conservation laws for mass, momentum and energy and to extrapolate characteristic curves. The conservation laws for a blade row are derived by integrating equations (1)–(3) over a rectangular domain covering the blade row. Restricting ourselves to a quasi-stationary transfer, that means we neglect the time derivatives, and letting the axial distance between the left and right boundary go to zero we obtain

$$\rho_r u_r - \rho_l u_l = f_\rho, \tag{10}$$

$$\rho_r u_r^2 + p_r - (\rho_l u_l^2 + p_l) = f_u, \tag{11}$$

$$\rho_r u_r v_r - \rho_l u_l v_l = f_v, \tag{12}$$

$$u_r(E_r + p_r) - u_l(E_l + p_l) = f_E, \tag{13}$$

where the indices l and r describe the left and right side of the blade row, and f_ρ, f_u, f_v, f_E are source terms for mass, momentum and energy for the blade row under consideration. While there is no source term for mass, the source terms for momentum and energy are calculated as a function of mass flow at time-step n

$$\dot{m}^n := 0.5(\rho_l^n u_l^n + \rho_r^n u_r^n)$$

($\rho_i^n, u_i^n, i = l, r$ are values for density and axial velocity at time n from the simulation) by

$$f_u(\dot{m}^n) := \rho_r u_r^2 + p_r - (\rho_l u_l^2 + p_l), \quad f_v(\dot{m}^n) := \rho_r u_r v_r - \rho_l u_l v_l,$$

$$f_E(\dot{m}^n) := u_r(E_r + p_r) - u_l(E_l + p_l),$$

where ρ_i, u_i, v_i and E_i $(i = l, r)$ are values from the compressor characteristic for the corresponding mass flow $\dot{m}^n$ (see Tables A3 and A4). By linearizing equations (1)–(3) over boundary values at time-step n we calculate characteristic variables for disturbances of these boundary values (see equation (8)) $\mathbf{c}_1, \mathbf{c}_2, \mathbf{c}_3$ on the left and $\mathbf{c}_4$ on the right boundary by extrapolating from the interior. In order to determine $\mathbf{c}_1$, $\mathbf{c}_2$, $\mathbf{c}_3$ on the left and $\mathbf{c}_4$ on the right boundary at time-step $n + 1$ we have to solve a polynomial equation of third order. While the Euler equations of gas dynamics do not take into account any effects of viscosity, in our model the effects of viscosity are captured by source terms for energy, which are positive for rotors and negative for stators. Therefore, the compressor model is a dissipative dynamical system, that means a dynamical system with loss of energy, which is compensated by source terms for energy. In order to take into consideration the time delay influence of blade rows we use a simple ODE

$$\omega + \tau \frac{\mathrm{d}\omega}{\mathrm{d}t} = \omega_s, \tag{14}$$

where τ denotes the delay time, the time for the gas to pass a blade row and ω_s denotes the final state, obtained from the transfer relation. In addition, the effect of rotation of the rotor has been considered by introducing a delay in space in the circumferential direction. The number of blades has been captured in the calculation by averaging over those circumferential grid points belonging to one passage and applying the transfer function to the averaged values.

4. INSTABILITIES AND BIFURCATIONS

The solution behaviour of our model is determined by the values for $\hat{\rho}_l$, $\hat{u}_l$, $\hat{v}_l$, $\hat{p}_l$ at the inlet and $\hat{\rho}_r$, $\hat{u}_r$, $\hat{v}_r$, $\hat{p}_r$ at the outlet of the compressor over which equation (5) has been linearized to formulate nonreflecting boundary conditions. By means of the compressor characteristic

TABLE 1
Overview of the different solution branches

Branch	Interval of stability for $\hat{p}_r$ (kPa) and $\dot{m}$ (% of DMF)		Remarks
Steady state	167–170	102.01–101.77	Time independent flow
Rotating stall-1	170–199	101.77–98.52	2 Cells, 150 Hz
Rotating stall-2	182–199	101.08–98.52	3 Cells, 150 Hz
Rotating stall-3	192–199	100.03–98.52	4 Cells, 150 Hz
Rotating pressure oscillations	199–205	98.52–96.86	1 Cell, 150 Hz, 600 Hz
Surge	205–208		5 Hz

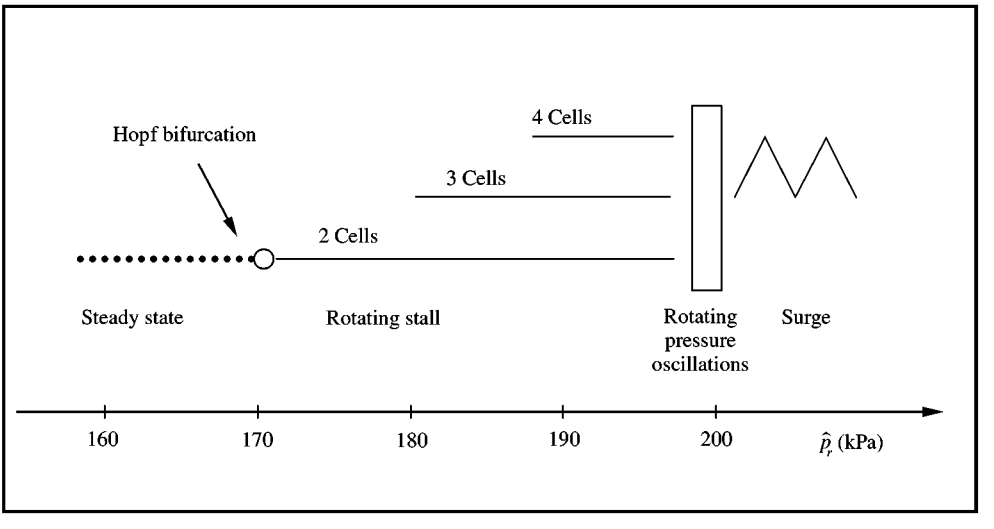

Figure 1. Schematic bifurcation diagram.

we can represent $\hat{\rho}_r$, $\hat{u}_r$ and $\hat{v}_r$ in terms of the exit pressure $\hat{p}_r$, thus $\hat{p}_r$ has been our bifurcation parameter. By changing $\hat{p}_r$ we have changed $\hat{\rho}_r$, $\hat{u}_r$, $\hat{v}_r$ and the mass flow $\dot{m}$ through the compressor. In the following, we describe the solution behaviour of our model if $\dot{m} = \dot{m}(\hat{p}_r)$ is reduced step by step ($\hat{p}_r$ is increased) starting with one selected value for exit pressure $\hat{p}_r = 167\,\text{kPa}$ for which the mass flow $\dot{m}$ is 102.01% of design mass flow (DMF). With increasing exit pressure a primary stable steady state loses stability to periodic solutions with a number of stall cells followed by rotating pressure oscillations and finally surge if the exit pressure is sufficiently large. The transition to surge is described in this chapter and an overview of all solution branches we found is given in Table 1 and presented schematically in Figure 1.

4.1. Bifurcation of Steady States and Rotating Stall

If we choose $\hat{p}_r \approx 167\,\text{kPa}$ we obtain a stable steady-state solution, the solution given by the compressor characteristic. All system trajectories are attracted by this solution. The flow converges to a state which is independent of time and space in every single region of the whole domain. For sufficiently large mass flow (low exit pressure $\hat{p}_r$) this steady-state solution is the only attracting state. We have transformed our model into a time discrete

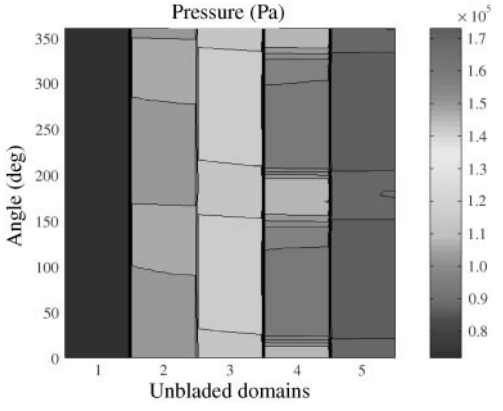

Figure 2. Pressure in the compressor for a periodic solution with two rotating stall cells behind every blade row moving in circumferential direction, $\hat{p}_r = 172.16\,\text{kPa}$.

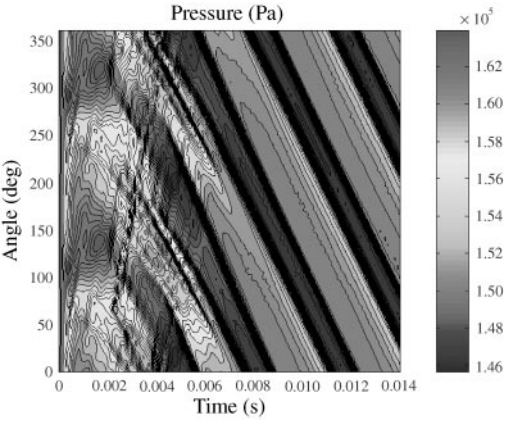

Figure 3. Pressure at compressor exit versus time, $\hat{p}_r = 172.16\,\text{kPa}$.

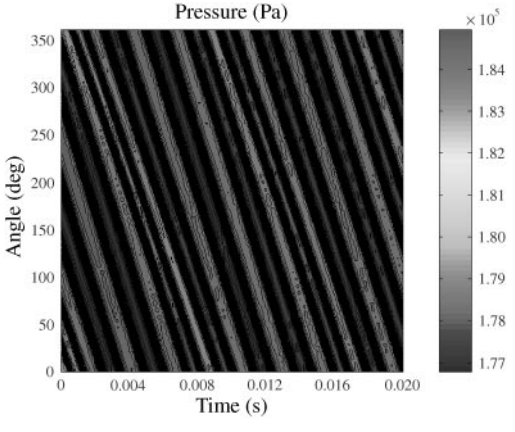

Figure 4. Pressure at compressor exit versus time, $\hat{p}_r = 182.22\,\text{kPa}$.

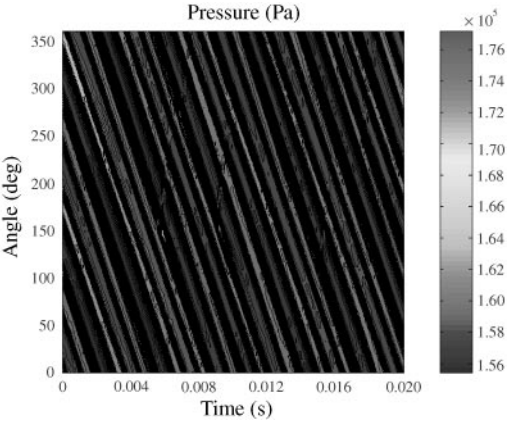

Figure 5. Pressure at compressor exit versus time, $\hat{p}_r = 192.08\,\text{kPa}$.

dynamical system of the form $x_{n+1} = f(x_n)$, where the steady state is a fixed point of f. For increasing exit pressure we have traced this steady solution branch. In each step of the tracing, in order to detect bifurcation points, the eigenvalues of the Jacobian matrix of f have been calculated. If the exit pressure is larger than a critical value, $\hat{p}_r \approx 170\,\text{kPa}$, the norm of one pair of complex conjugate eigenvalues exceeds 1. The steady-state losses its stability by a Hopf bifurcation to a time-periodic state with two rotating stall cells in every single unbladed region.

In Figure 2, the pressure in the five unbladed regions of the compressor is given for just one point in time if $\hat{p}_r$ is slightly above this critical value. Behind every blade row there are two stall cells moving in circumferential direction. In Figure 3, the instability of the steady state is demonstrated for $\hat{p}_r = 172.16\,\text{kPa}$. The pressure at the compressor exit is plotted versus time. It can be seen how the flow at the compressor exit escapes the originally stable steady state and approaches a new periodic orbit with two moving stall cells. The number of stall cells in the new periodic state depends on the pressure at the exit. For $\hat{p}_r \approx 182\,\text{kPa}$ a new periodic solution with three stall cells and for $\hat{p}_r \approx 192\,\text{kPa}$ a periodic solution with

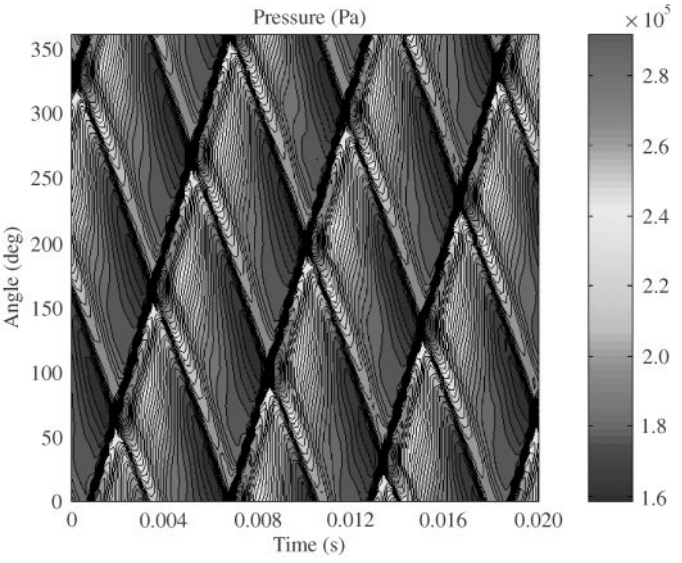

Figure 6. Pressure at compressor exit versus time, $\hat{p}_r = 199.74\,\text{kPa}$.

four stall cells appear. In Figures 4 and 5 the exit pressure is plotted versus time for stable periodic solutions with three and four stall cells. The branch with two stall cells remains stable. Thus, altogether three stable periodic solutions coexist.

The sense of rotation of the stall cells corresponds to that of the rotor and the rotation frequency is approximately 150 Hz which is about 60% of that of the rotor. The pressure in the stall cells does not depend on time. For these flows the mass flow and the averaged pressure in every unbladed domain does not depend on time, i.e., these flows include no effects of surge. All solution branches lead to a solutions with time-periodic oscillation of the pressure in the stall cells, if the exit pressure is increased further and finally to surge, i.e., an oscillation of mass flow in time.

4.2. Rotating Pressure Oscillations

For $\hat{p}_r \approx 199\,\text{kPa}$ the periodic solutions with stall cells disappear and a new solution occurs with two cells, whose pressure oscillates in time. Both cells are moving in circumferential direction with opposite sense of rotation what can be seen in Figure 6.

In contrast to the rotating stall solutions, where the pressure in the cells remains constant, now the pressure oscillates in time. The mass flow for this solution remains time independent. The rotation frequency of the stall cell is again 150 Hz and the frequency of the pressure oscillation is approximately 600 Hz.

A similar form of instability has been observed experimentally by Kameier & Diederen (1996) and it was called the rotating instability. According to Kameier and Diederen, rotating instabilities result from rotating source mechanisms in the blade tips of the rotor. The difference to rotating stall is that the pressure in the rotating cells is not constant. Due to the separation of eddies from the surface of the blades circumferential modes of high order are generated. The correspondence of the frequency of the perturbation and the blade passing frequency (BPF) may lead to an increase of sound and to blade oscillations of high amplitudes (Kameier 1994). This is of course a 3-D effect, which is not included in our simulation.

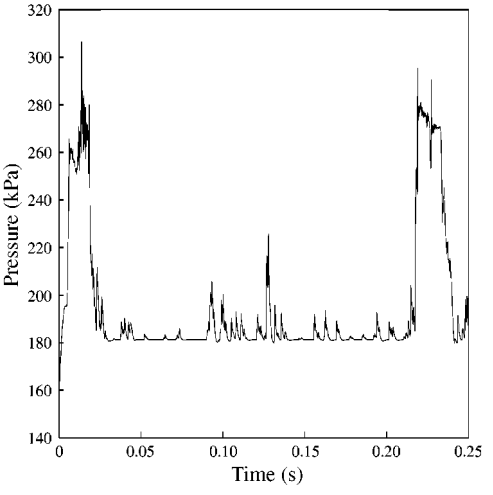

Figure 7. Averaged pressure behind rotor 2 versus time, $\hat{p}_r = 205.11\,\text{kPa}$.

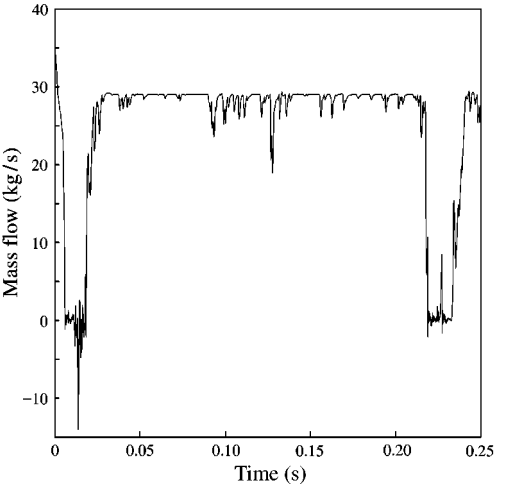

Figure 8. Mass flow behind rotor 2 versus time, $\hat{p}_r = 205.11\,\text{kPa}$.

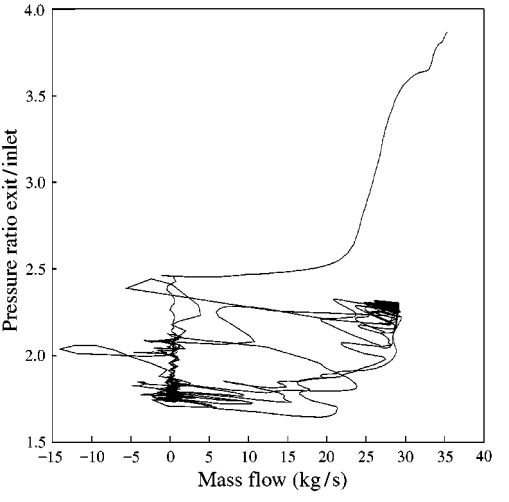

Figure 9. Movement of point of operation in the plane mass flow/pressure ratio, $\hat{p}_r = 205.11\,\text{kPa}$.

4.3. Surge

Finally, if the pressure at the exit is increased further, $\hat{p}_r \geq 205\,\text{kPa}$, all solutions branch with stall cells and rotating stall cells become instable and a solution occurs with variation of mass flow in time.

We observed a high-pressure wave, which propagates in axial direction from the compressor exit to the entrance. In Figures 7 and 8, the averaged pressure and the mass flow at the exit of the compressor is given versus time. A peak of high pressure is coupled with a decrease of mass flow, the mass flow becomes negative, followed by a period of irregular behaviour until the next surge period starts. The frequency is approximately 5 Hz. Figure 9 shows the movement of the point of operation in the plane mass flow/pressure ratio. The

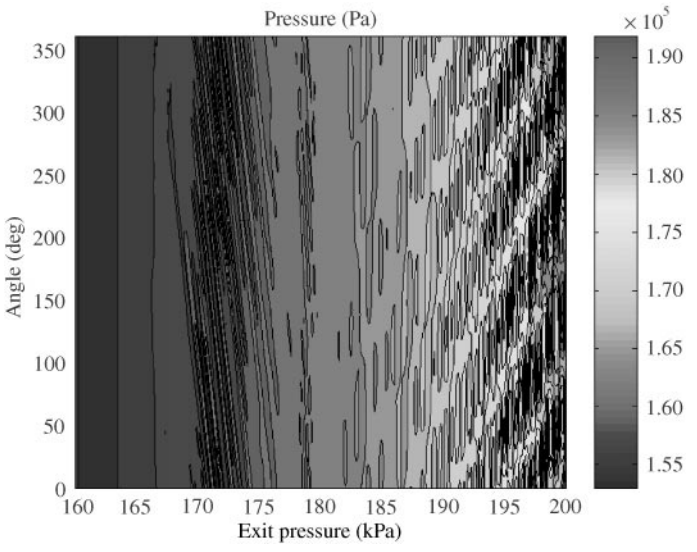

Figure 10. Pressure at compressor exit versus imposed exit pressure for a throttled compressor.

mass flow decreases to zero followed by a decrease of pressure ratio between exit and inlet until the mass flow and pressure ratio increase again.

4.4. Throttling of the Compressor

In this part of the calculation we have increased the exit pressure while calculating the evolution of the flow in time, that means we have throttled the compressor. The flow is calculated for a time period of 0.07 s and the exit pressure $\hat{p}_r$ is increased during this period of time from 160 to 200 kPa and the mass flow is reduced from 102.01 to 96.86% of DMF. In Figure 10, the pressure at the exit of the compressor is given versus the imposed exit pressure $\hat{p}_r$. We observed that the state of the compressor changes. For $\hat{p}_r = 160$ kPa we start with $\dot{m} = 102.01\%$ of DMF with a regular flow without any disturbances. For $\hat{p}_r = 170$ kPa spikes incept, which disappear followed by rotating stall cells for $\hat{p}_r = 175$ kPa.

These stall cells disappear after a period of approximately 0.01 s. Spikes appear again for $\hat{p}_r = 185$ and 195 kPa stall cells appear with oscillating pressure.

5. COMPARISON OF NUMERICAL SIMULATION WITH MEASURED DATA

The simulation results are now compared with test results from the compressor under consideration, which have been recorded by Kameier (1997). The data are taken from the 10-stage high-pressure compressor (HPC) of the BR710 jet engine, while the numerical simulation is done for the first two stages. Several compressor stall and surge events are systematically analysed by means of fast responding pressure measurements. Three equally spaced pressure sensors were distributed along the circumference near the leading edge of every rotor. The time and spatial resolution of the pressure data are limited by the available recording system, what affects the comparison between experimental and calculated data.

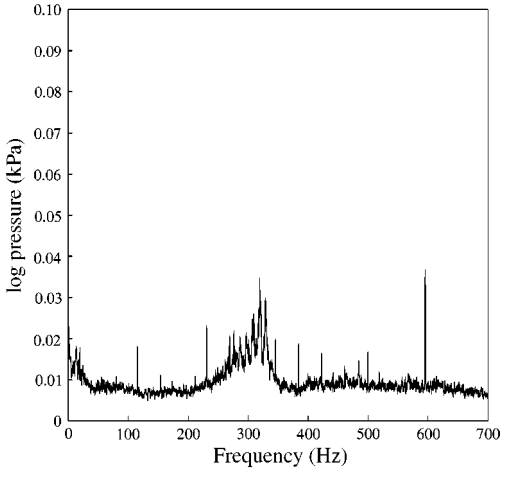

Figure 11. Frequency spectrum of pressure signals behind rotor 1.

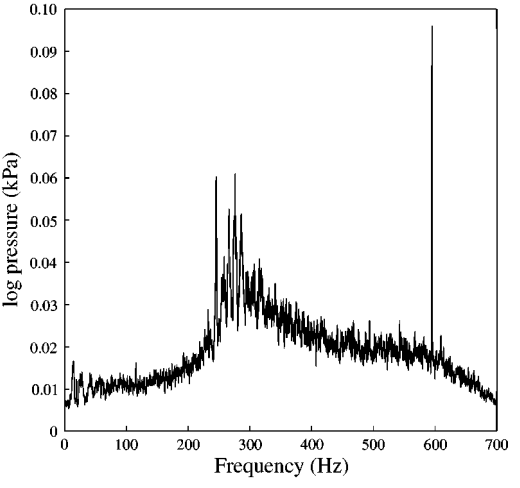

Figure 12. Frequency spectrum of pressure signals behind rotor 2.

5.1. Summary of Rotating Stall Results from HPC Rig

For a large tip clearance ratio rotating stall and rotating pressure oscillations have been observed near the instability point. Inception of rotating stall appears at 0.97% of design mass flow.

Figures 11 and 12 show frequency spectra of the pressure signatures behind rotors 1 and 2 of these sensors for a mass flow near the instability point. There are two main frequencies. The frequency of rotating stall oscillations is a little larger than 300 Hz for rotor 1 and a little smaller than 300 Hz for rotor 2 and the frequency of rotating pressure oscillations, which result from large tip clearance ratios is about 600 Hz. These values are similar to the numerical simulation results. Although our numerical simulations are two-dimensional and we therefore are not able to locate the rotating pressure oscillations of the numerical results at the tips of the blades, there are some qualitative similarities between numerical and experimental results, namely the oscillation of pressure in the stall cells.

5.2. Summary of Surge Results from HPC Rig

If the mass flow undergoes a critical value, surge oscillations have been observed. Figure 13 shows a pressure signal for a surge event behind rotor 1. Inception of surge is at 0.92% of design mass flow. The frequency of measured surge oscillations is nearly 2 Hz, what is a little smaller than in the numerical simulation.

The systematic analysis of measurements in the compressor rig operating in unstable conditions up to surge support the following understanding of the instability mechanisms (Kameier 1997). The surge shock wave is propagating as a nonplanar wave through the compressor. The flow direction right after the surge is upstream which causes a large temperature increase in the front stages. The time between the occurrence of the trigger and the surge event is very short. For detailed conclusions and comparison with numerical simulations the instrumentation is too sparse. The numerical simulations have a high time and space location resolution. Especially the circumferential distribution of several transducers on the same axial position would be beneficial for a better comparison.

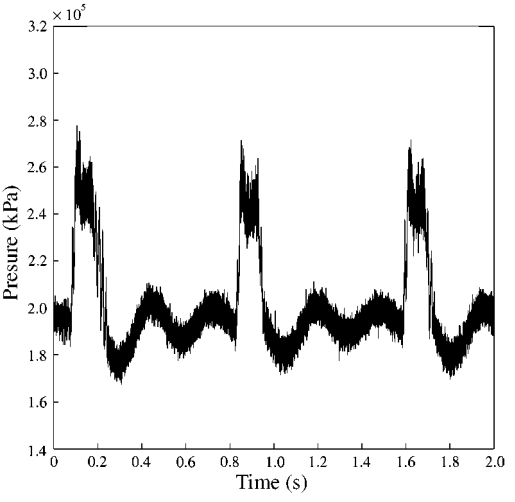

Figure 13. Pressure versus time behind rotor 1.

6. CONCLUSION

In this paper, we have numerically investigated the effects of throttling the compressor to flowfield instabilities. The compressor model presented here is able to describe the qualitative transition behaviour of the flow from the inception process of rotating stall to surge. It has been shown that the flow undergoes several qualitative changes if the imposed exit pressure is increased and the mass flow through the compressor is reduced. We start with a steady-state solution if the mass flow through the compressor is sufficiently large. For an exit pressure slightly above the first critical value we observed coexisting solution branches with 2, 3 and 4 rotating stall cells. These branches lead to states with pressure oscillations in the stall cells and finally surge, i.e., solutions with mass flow periodic in time, when the exit pressure is sufficiently large. The rotating stall and surge phenomena could also be found in the experimental investigations. The transition to surge seems to follow a scenario found by Day, namely surge appears after an initial period of rotating stall. Furthermore, we found that the scenario leading to surge is similar to the transition to irregular behaviour observed in many problems of hydrodynamics. A primary steady state losses stability to a time-periodic state followed by a state with two frequencies and finally irregular turbulent behaviour. Although we use Euler equations to simulate the flow in the unbladed regions, our model takes into account the effects of viscosity by transfer conditions. Comparison of numerical simulation results with experimental data have shown that the model is able to describe the rotating stall and surge phenomena found in the experimental data. A more detailed investigation of the relations between instabilities and design parameters is still necessary to fully understand the physical phenomena.

7. ACKNOWLEDGEMENTS

This work has been done at the Weierstrass Institute (WIAS) Berlin and was supported in part by the BMW Rolls-Royce GmbH and in part by the BMBF under its main topic "Arbeitsgemeinschaft Hochtemperatur-Gasturbine" under grant 327040L. Furthermore, we would like to thank BMW Rolls-Royce for experimental data of the compressor under consideration.

References

ANDERSON, D. A., TANNEHILL, J. C. & PLETCHER, R. H. 1984 *Computational Fluid Mechanics and Heat Transfer*. New York. Hemisphere Publishing Corporation.

BREUER, T. 1995 Theoretische Untersuchung des instationären Betriebsverhaltens transoni-scher Axialverdichter an der Stabilitätsgrenze. *Abschlußbericht HTGT - Turbotech*, *Arbeitspaket No.* 1.1.1.11.

BREUER, T. 1996 Theoretische Untersuchung des instationären Betriebsverhaltens transoni-scher Verdichter an der Stabilitätsgrenze. *Abschlußbericht HTGT - Turbotech Interim*, *Arbeitspaket No.* 1.240.

BRØNS, M. 1988 Bifurcations and instabilities in the Greitzer model for compressor system surge. *Mathematics in Engineering and Industry*, **2,** 51–63.

BRØNS, M. 1990 A model for compressor flow instability with mode shifting. *Mathematical Computer Modelling*, **14,** 746–749.

COURANT, R. & FRIEDRICHS, K. O. 1976 *Supersonic Flow and Shock Waves*. New York: Springer.

CORDES, G. 1963 *Strömungstechnik der gasbeaufschlagten Axialturbine*. Berlin: Springer.

DAY, I. J., 1993 Stall inception in axial flow compressors. *ASME Journal of Turbomachinery* **115,** 1–9.

DAY, I. J., 1994 Axial compressor performance during surge. *ASME Journal of Populsion and Power* **10,** 329–336.

DEMARGNE, A. A. J. & LONGLEY, J. P. 1997 Comparisons between measured and calculated stall development in four high-speed multi-stage compressors. *Proceedings*, *ASME Turbo Expo '97*, *Land*, *Sea and Air*, *42nd Gas Turbine and Aeroengine Congress*, *User's Symposium and Exposition*, Orlando, FL, U.S.A., ASME Paper 97-GT-467.

ENGQUIST, B. & MAJDA, A. 1977 Absorbing boundary conditions for the numerical simulation of waves. *Mathematics of Computation*, **31,** 629–651.

EMMONS, H. W., PEARSON, C. E. & GRANT, H. P. 1955 Compressor surge and stall propagation. *Transactions of the ASME* **77,** 455–469.

GRAVDAHL, J. T. & EGELAND, O. 1999 *Compressor Surge and Rotating Stall*. London: Springer.

GILES, M. 1990 Nonreflecting boundary conditions for Euler equation calculations. *AIAA Journal* **28,** 2050–2057.

GREITZER, E. M. & MOORE, F. K. 1986 A theory of post-stall transients in axial compression systems, Part 2: Application. *ASME Journal of Engineering for Gas Turbines and Power* **108,** 231–239.

GRAVDAHL, J. T. 1998 Modeling and control of surge and rotating stall in compressors. Ph.D. Thesis, Norwegian University of Science and Technology.

GREITZER, E. M. 1976*a* Surge and rotating stall in axial flow compressors, Part 1: Theoretical compression system model. *ASME Journal of Engineering for Power* **98,** 190–198.

GREITZER, E. M. 1976*b* Surge and rotating stall in axial flow compressors, Part 2: Experimental results and comparison with theory. *ASME Journal of Engineering for Power* **98,** 199–217.

GREITZER, E. M. 1981 the stability of pumping systems — the 1980 Freeman Scholar Lecture. *ASME Journal of Fluids Engineering* **102,** 139–242.

KAMEIER, F. 1994 Experimentelle Untersuchung zur Entstehung und Minderung des Blattspit-zen–Wirbellärms axialer Strömungsmaschinen. *Fortschritt—Berichte VDI*, Reihe 7 No. **243,** Düsseldorf.

KAMEIER, F. 1997 Surge investigation on a 10-stage high speed compressor rig. BMW Rolls-Royce Technical Report E-TR044/97.

KAMEIER, F. & DIEDEREN, W. 1996 Aerodynamic investigation of rotating instabilities in BR710 HPC Rotor 1. BMW Rolls-Royce Technical Report E-TR063/96.

LIAW, D. C. & ABED, E. H. 1996 Active control of compressor stall inception: a bifurcation-theoretic approach. *Automatica* **32,** 109–115.

LEVEQUE, R. J. 1990 *Numerical Methods for Conservation Laws*. Basel: Birkhäuser.

LEVEQUE, R. J. 1994 CLAWPACK — a software package for solving multidimensional conservation laws. *Proceedings of the 5th International Conference on Hyperbolic Problems*: *Theory*, *Numerics*, *Applications* (eds J. Glimm *et al.*) Singapore: World Scientific.

LEVEQUE, R. J. 1997 Wave propagation algorithms for multi-dimensional hyperbolic systems. *Journal of Computational Physics* **131,** 327–353.

LEWIS, R. I. 1996 *Turbomachinery Performance Analysis*. London: Arnold.

LONGLEY, J. P. 1994 A review of non-steady flow models for compressor stability. *ASME Journal of Turbomachinery* **116,** 202–215.

LONGLEY, J. P. 1996 Advanced civil core compressor aerodynamics. Brite/Euram AC3A Project, Task B6.

LONGLEY, J. P. 1997 Calculating the flowfield behaviour of high-speed multi-stage compressors. *Proceedings, ASME Turbo Expo* 97, *Land, Sea and Air*, 42*nd Gas Turbine and Aeroengine Congress, User's Symposium and Exposition*, Orlando, FL, U.S.A., ASME Paper 97-GT-468.
MCCAUGHAN, F. E. 1989 Application of bifurcation theory to axial flow compressor instability. *ASME Journal of Turbomachinery* **111,** 426–433.
MCDOUGALL, N. M., CUMPSTY, N. A. & HYNES, T. P. 1990 Stall inception in axial compressors. *ASME Journal of Turbomachinery* **112,** 116–125.
MOORE, F. K. & GREITZER, E. M. 1986 A theory of post-stall transients in axial compression systems, Part 1: Development of equations. *ASME Journal of Engineering for Gas Turbines and Power* **108,** 68–76.
MERZ, R., MAYER, J. F. & STETTER, H. 1996 Navier–Stokes für axiale Turbinenstufen. Arbeitsbericht zum Forschungsvorhaben Ste 489/1-2, Universität Stuttgart.
WILCOX, D. C. 1993 *Turbulence Modeling for CFD*, La Cañada: DCW Industries, Inc. 2nd edition.

APPENDIX

In Tables A1 and A2 the geometry and the design parameters of the two-stage compressor under consideration for numerical investigation is given. Tables A3 and A4 contain the compressor characteristic. The used symbols are given below.

α	angle	0	inlet rotor absolute system
MNS/MNR	Mach number stator/rotor	1	inlet rotor relative system
T	total temperature	2	exit rotor relative system
DT	difference in total temperatures (exit − inlet)	3	inlet stator absolute system
		4	exit stator absolute system
PS/PT	static/total pressure		
DMF	design mass flow		
$\dot{m}$	mass flow		

TABLE A1
Compressor geometry

Stage	Axial position (m)	Radius in (m)	Radius out (m)
	0.0000	0.1348	0.2615
	0.0441	0.1348	0.2615
1	0.0882	0.1415	0.2558
	0.1009	0.1415	0.2558
	0.1561	0.1553	0.2489
	0.1685	0.1553	0.2489
2	0.2111	0.1692	0.2458
	0.2208	0.1692	0.2458
	0.2583	0.1784	0.2435
	0.2653	0.1784	0.2435

TABLE A2
Design parameters for a two-stage compressor

No. of rotor blades stage 1/2	32/50
No. of stator blades stage 1/2	31/38
Reynolds number at rotor inlet	5.1×10^6
Mach number at rotor inlet	0.744
Design speed	14636.36/min
Design mass flow (DMF)	33.19 kg/s

TABLE A3
Compressor characteristic; stages 1 and 2

Stage	$\dot{m}$ (% of DMF)	α_1 (deg)	α_2 (deg)	α_3 (deg)	α_4 (deg)	MNR	MNS	DT/T0
	95.05	53.28	33.32	46.37	9.50	1.024	0.744	0.160
	96.86	52.30	33.12	45.41	9.26	1.035	0.750	0.175
	98.52	51.34	33.00	44.22	9.05	1.047	0.757	0.153
1	100.00	50.49	32.95	43.04	8.95	1.059	0.763	0.149
	101.08	49.80	32.91	41.94	8.92	1.068	0.769	0.145
	101.77	49.36	32.88	41.15	8.90	1.075	0.774	0.142
	102.01	49.20	32.87	40.86	8.90	1.077	0.776	0.141
	95.05	55.92	33.36	46.18	12.51	0.969	0.721	0.154
	96.86	55.28	33.22	45.25	12.28	0.980	0.727	0.152
	98.52	54.49	33.10	44.09	12.09	0.992	0.734	0.150
2	100.00	53.58	33.02	42.67	12.01	1.006	0.742	0.147
	101.08	52.66	32.98	41.06	11.97	1.019	0.752	0.142
	101.77	51.93	32.92	39.54	11.92	1.029	0.763	0.138
	102.01	51.66	32.89	38.89	11.90	1.033	0.767	0.136

TABLE A4
Compressor characteristic; stages 1 and 2

Stage	$\dot{m}$ (% of DMF)	PS0 (kPa)	PS3 (kPa)	PS4 (kPa)	PT0 (kPa)	PT3 (kPa)	PT4 (kPa)	T0 [K]
	95.05	78.04	112.59	130.03	101.35	162.50	159.82	288.15
	96.86	76.73	111.35	128.10	101.35	161.68	159.20	288.15
	98.52	75.35	109.48	125.27	101.35	160.02	157.75	288.15
1	100.00	74.04	107.42	121.69	101.35	157.89	155.68	288.15
	101.08	73.01	105.28	117.90	101.35	155.68	153.47	288.15
	101.77	72.32	103.69	114.93	101.35	154.02	151.68	288.15
	102.01	72.11	103.07	113.83	101.35	153.40	150.99	288.15
	95.05	130.03	179.67	208.22	159.82	253.93	249.86	334.20
	96.86	128.10	177.47	205.11	159.20	252.21	248.48	333.29
	98.52	125.27	173.74	199.74	157.75	248.55	245.17	332.14
2	100.00	121.69	168.57	192.08	155.68	242.97	239.79	330.98
	101.08	117.90	162.30	182.22	153.47	236.14	232.90	329.89
	101.77	114.93	156.30	172.16	151.68	229.59	225.73	329.13
	102.01	113.83	153.68	167.40	150.99	226.83	222.49	328.85